Received: 29 June 2018 | Revised: 13 September 2018 | Accepted: 14 September 2018

DOI: 10.1002/dta.2508

RESEARCH ARTICLE

WILEY

Suspect and non-target screening workflows to investigate the *in vitro* and *in vivo* metabolism of the synthetic cannabinoid 5Cl-THJ-018

Philippe Vervliet[1] | Olivier Mortelé[1] | Celine Gys[1] | Maarten Degreef[1] | Katrien Lanckmans[2] | Kristof Maudens[1] | Adrian Covaci[1] | Alexander L.N. van Nuijs[1] | Foon Yin Lai[1]

[1] Toxicological Centre, University of Antwerp, Antwerp, Belgium

[2] Universitair Ziekenhuis Brussel, Jette, Belgium

Correspondence
Philippe Vervliet and Alexander L. N. van Nuijs, Toxicological Centre, University of Antwerp, Universiteitsplein 1, 2610 Antwerp, Belgium.
Email: philippe.vervliet@uantwerpen.be; alexander.vannuijs@uantwerpen.be.

Funding information
Directorate-General for Research and Innovation, Grant/Award Number: 692241; Fonds Wetenschappelijk Onderzoek, Grant/Award Numbers: G089016N and G0E5216N; H2020 Marie Skłodowska-Curie Actions, Grant/Award Number: 749845 APOLLO; Universiteit Antwerpen, Grant/Award Number: GOA project

Abstract

The use of synthetic cannabinoids causes similar effects as Δ^9-tetrahydrocannabinol and long-term (ab)use can lead to health hazards and fatal intoxications. As most investigated synthetic cannabinoids undergo extensive biotransformation, almost no parent compound can be detected in urine, which hampers forensic investigations. Limited information about the biotransformation products of new synthetic cannabinoids makes the detection of these drugs in various biological matrices challenging. This study aimed to identify the main *in vitro* biotransformation pathways of 5Cl-THJ-018 and to compare these findings with an authentic urine sample of a 5Cl-THJ-018 user. The synthetic cannabinoid was incubated with pooled human liver microsomes and cytosol to simulate phase I and phase II biotransformations. Resulting extracts were analyzed with liquid chromatography coupled to quadrupole time-of-flight mass spectrometry (LC–QTOF–MS). Three different data analysis workflows were applied to identify biotransformation products. A suspect screening workflow used an in-house database built from literature data and *in silico* biotransformation predictions. Two non-target screening workflows used a commercially available software and an open-source software for mass spectrometry data processing. A total of 23 *in vitro* biotransformation products were identified, with hydroxylation, oxidative dechlorination, and dihydrodiol formation pathways as the main phase I reactions. Additionally, five glucuronidated and three sulfated phase II conjugates were identified. The predominant *in vivo* pathway was through oxidative dechlorination and in total six metabolites of 5Cl-THJ-018 were identified. Biotransformation products both *in vitro* and *in vivo* were successfully identified using complementary suspect and non-target screening workflows.

KEYWORDS

cytosolic fractions, human liver microsomes, *In vitro* biotransformation, liquid chromatography-mass spectrometry, new psychoactive substances

Philippe Vervliet and Olivier Mortelé joint first authors.

1 | INTRODUCTION

In recent years, new psychoactive substances (NPS) have been increasingly released into the drug market and are often easily accessible via the Internet. One of the most important NPS classes is the group of the synthetic cannabinoids (SCs), which contains mostly substances of high potency and seems to be establishing a foothold in the drug market since their first appearance in the early to mid-2000s.[1-4] SCs and some of their metabolites mimic the effects of Δ^9-tetrahydrocannabinol (the major psychoactive component found in cannabis) by a high affinity interaction with the cannabinoid type 1 (CB1) and type 2 (CB2) receptors.[2,5-8] Consumption of SCs has increased and led to the implementation of control measures across the European Union regarding an increasing number of new SCs.[4,9]

As most investigated SCs are prone to extensive biotransformation, parent compounds are rarely detected in urine. Without knowledge of their biotransformation products, forensic investigations on the use of these substances can be impeded. Since information about biotransformation products of novel SCs is very limited to unavailable, the detection of these illicit drugs in various biological matrices can be challenging.[5,7,8,10-12]

The SC 5Cl-THJ-018 [(1-(5-chloropentyl)-1H-indazol-3-yl)(naphthalen-1-yl)methanone] is a new SC with a napthoylindazole structure, derived from THJ-018 by addition of a chlorine on the pentyl side chain. Human metabolism of a number of structurally related SCs has been evaluated in different settings, but to our best knowledge, this information is missing for 5Cl-THJ-018.[10,11,13-17]

Pooled human liver microsomes (HLMs) are a suitable source of enzymes for examining *in vitro* human metabolism as they contain the major drug-metabolizing enzymes: The cytochrome P450 isoenzymes (CYPs) and UDP-glucuronosyltransferases (UGTs).[18-21] Complementary to HLMs, human liver cytosol (HLCYT) contains sulfotransferase (SULT) and can be used to study *in vitro* sulfation reactions.

The aims of this study were to identify the main phase I and phase II *in vitro* biotransformation products of 5Cl-THJ-018, and to compare these *in vitro* findings with an urine sample of a 5Cl-THJ-018 user in order to propose potential, reliable and specific biomarkers for the detection of this SC. To do so, 5Cl-THJ-018 was incubated with HLMs, HLCYT, and suitable cofactors to simulate phase I[22] and phase II[23] biotransformation reactions. Liquid chromatography coupled to high-resolution accurate-mass quadrupole-time-of-flight mass spectrometry (LC–QTOF–MS) and three complementary data analysis workflows were used to screen, identify and elucidate biotransformation products formed in the *in vitro* assay and metabolites present in the urine sample.

2 | MATERIALS AND METHODS

2.1 | Chemicals and reagents

5Cl-THJ-018 was acquired from Cayman Chemical (Ann Arbor, MI, USA). HLMs (mixed gender, n = 50) were acquired from Tebu-Bio (Boechout, Belgium). HLCYT (mixed gender, n = 150), theophylline (anhydrous, > 99 %), 2,5-uridinediphosphate glucuronic acid (UDPGA), adenosine-3′-phosphate 5′-phosphosulfate (PAPS, > 60 %) lithium salt hydrate, alamethicin (neat, > 98 %), dimethyl sulfoxide (DMSO), and 4-nitrophenol (4-NP) were obtained from Sigma-Aldrich (St Louis, MO, USA). NADPH tetrasodium salt hydrate (> 96 %) was purchased from Acros (Geel, Belgium). Acetonitrile (ACN, HPLC-grade) and methanol (MeOH, ≥ 99.9 % LC–MS grade) were acquired from Fisher Chemical (Loughborough, UK), formic acid (> 98 %) and hydrochloric acid (37 %) from Merck KGaA (Darmstadt, Germany). A 100 mM TRIS-buffer was prepared by dissolving 12.11 g Trizma base (Janssen Chimica, Beerse, Belgium) and 1.02 g $MgCl_2$ (Merck KGaA, Darmstadt, Germany) in 1 L ultrapure water. The pH was adjusted to 7.4 by adding 1 M HCl solution. Ultra-pure water was produced in-house with a PURELAB-purifier system of Elga Labwater (Tienen, Belgium).

2.2 | *In vitro* metabolism assay

This study employed the *in vitro* assay optimized and used in previous studies.[23-27] An overview of the experimental setup can be found in the Supporting Information (Figure SI-1). All tested sample sets contained three replicates.

2.2.1 | Phase I incubations

Phase I biotransformation products were generated using pooled HLMs. A reaction mixture containing 945 µL of TRIS-buffer (pH 7.4, 100 mM), 25 µL of HLMs (20 mg/mL in 250 mM sucrose in water) and 10 µL of 5Cl-THJ-018 stock solution (0.5 mM in MeOH) was incubated in a 1.5 mL Eppendorf tube at 37 °C. 10 µL of NADPH (0.1 M in TRIS-buffer) was added after 5, 60 and 120 minutes. During incubation the total volume of organic solvent did not exceed 1 % in order to avoid any effects on the microsomal activity.[22] Three negative control samples (without 5Cl-THJ-018, HLMs or NADPH) were prepared in parallel. The reaction was stopped after 1 h or 3 hours by the addition of 250 µL ice-cold ACN containing 1 % formic acid (phase I experiments) or by putting the samples on ice for 3 minutes (samples for further phase II experiments). The internal standard, theophylline, was prepared in the ice-cold ACN with 1 % formic acid at 5 µg/mL. A positive control for phase I experiments was included by incubating 10 µL phenacetin (5 µg/mL in ultrapure water). The formation of two phase I biotransformation products - N-(4-hydroxyphenyl)-acetamide (P1) and N-(4-ethoxy-2-hydroxyphenyl)-acetamide (P2) was monitored.

2.2.2 | Phase II incubations

Following the phase I experiments, samples were exposed to phase II conjugation through glucuronidation (GLU) and sulfation (SUL). For the GLU samples, 935 µL of the supernatant originating from the phase I samples was incubated with 25 µL of HLMs and 10 µL of alamethicin (1 mg/mL in DMSO). Ten µL of UDPGA (100 mM in TRIS-buffer) was added after 5, 60, and 120 minutes. SUL samples consisted of a mixture of 965 µL supernatant and 25 µL cytosol (20 mg/mL in buffer containing 150 mM potassium chloride and 50 mM Tris, pH 7.5, with 2mM EDTA), with addition of 10 µL PAPs (10 mM in TRIS-buffer) after 5, 60, and 120 minutes of incubation. Negative control samples were prepared by omitting 5Cl-THJ-018 or the cofactor (UDPGA and PAPs) in order to exclude false-positive

results. A positive control was included by incubating 4-NP (10 µL of 10 mM in TRIS-buffer) and monitoring the formation of 4-NP glucuronide and 4-NP sulfate. Reactions were stopped as described earlier for the phase I incubations.

All samples were centrifuged for 5 minutes at 8000 rpm (5900 g). The supernatant was transferred to a clean glass tube, evaporated under nitrogen at 38 °C, and reconstituted in 200 µL of a 10 % (v/v) ACN in ultrapure water solution for LC–QTOF–MS analysis.

2.3 | *In vivo* urine sample

In early 2017, a 46-year-old man was brought to the emergency department of the hospital. His symptoms included hallucinations, depersonalization, auditory hallucinations, and pronounced disorientation, as well as constricted pupils. The patient was known for his drug addiction and had been using the cathinone 3-methylmethcathinon (3-MMC) daily up until three weeks before admission. On the day of admission, the patient had sniffed an unknown quantity of a powder bought on the Internet and believed to be methiopropamine. A urine sample was collected and screened negative for methiopropamine and its metabolites. Gas chromatography–mass spectrometry (GC–MS) screening using an extensive liquid–liquid extraction (LLE) clean-up (resulting in a 50-fold concentration increase) showed the presence of 5Cl-THJ-018, which was confirmed using the Cayman mass spectral library (v10312016). A description of the screening can be found in the Supporting Information.

To compare the identified *in vitro* biotransformation products with the *in vivo* metabolites, 50 µL of acetonitrile was added to 50 µL of the collected urine, vortexed for 30 seconds and transferred to a 0.2 µm nylon centrifugal filter (5 minutes at 8000 rpm (5900 g)) and analyzed with LC–QTOF–MS.

2.4 | LC–QTOF–MS analytical method

Extracts were analyzed using an Agilent 1290 Infinity UPLC hyphenated to an Agilent 6530 QTOF (Agilent, Santa Clara, CA, USA). Chromatographic separation was performed on a Kinetex C8 column (150 x 2.1 mm; 1.7 µm particle size, Phenomenex, Utrecht, Netherlands) using a mobile phase composed of ultra-pure water with 0.04 % (v/v) formic acid (A) and 80/20 (v/v) acetonitrile/ultrapure water with 0.04 % formic acid (v/v on total volume) (B) with a flow of 0.3 mL/min. The injection volume was 5 µL. All samples were analyzed in positive and negative ionization mode. The eluent was directed to the waste during the first minute of each run to protect the ion source from extensive contamination. The chromatographic run started with 2 minutes isocratic at 10 % B, after which a gradient was used to increase the percentage of B to 95 % at 20 minutes. The column was rinsed with 95 % B for 4 minutes and re-equilibrated at 10 % B for 5 minutes before the next injection. The column temperature was kept constant at 40 °C.

The QTOF–MS instrument was operated in the 2 GHz (extended dynamic range) mode, providing a Full Width at Half Maximum (FWHM) resolution of approximately 5100 at *m/z* 118.0862 and 10000 at *m/z* 922.0098. The ions *m/z* 112.0508 and 922.0097 for positive mode and *m/z* 112.9855 and 966.0007 for negative mode were selected for constant recalibration throughout the chromatographic run to ensure high mass accuracy. The eluting compounds were ionized using Agilent Jet-Stream electrospray ionization (ESI) in both positive and negative ionization mode. Drying gas temperature and flow were at 300 °C and 8 L/min, respectively. The sheath gas temperature was 350 °C at a flow of 11 L/min. Nebulizer pressure was set at 25 psig. Capillary, nozzle and fragmentor voltages were at 3500 V, 500 V and 120 V, respectively. The acquisition parameters were set for an *m/z* range from 75 to 1000 at a scan rate of 2.5 scans/s and 6.67 scans/s for MS and MS/MS spectra, respectively. Collision energies were applied at 10 and 20 V. Signals were detected using a data-dependent acquisition method. An active exclusion of 0.2 minutes was applied to prevent repetitive acquisition of MS/MS spectra for the same ion. All data were stored in centroid mode and exported for analysis.

2.5 | Workflows and data analysis

This study employed three different workflows for processing the acquired *in vitro* data (Figure SI-2). Next to a suspect screening based on *in silico* metabolite prediction, two different non-target screening workflows were conducted.

2.5.1 | Suspect screening workflow

The suspect screening workflow was based on an in-house developed workflow, which has been published previously.[26,28,29] First, a list of possible biotransformation products was generated using the Meteor Nexus (v2.1, Lhasa Limited, Leeds, UK) software. For phase I metabolism, all redox and non-redox biotransformations were selected. For phase II metabolism, *O*- and *N*-glucuronidation, *O*- and *N*-sulfation, acetylation and conjugation with amino acids were selected. The metabolite prediction was processed with human CYP enzymes, the maximum depth set on 3 and the maximum number of biotransformation products set at 1000. The generated list of possible biotransformation products with the molecular formula, exact mass, structure and related enzyme for the corresponding metabolism was stored as a csv-database. Furthermore, the metabolites of other similar cannabinoids, described in the literature and not predicted by the software, were added to the list.[13]

2.5.2 | MzMine + R workflow

A non-target screening approach was conducted with the metabolomics software MZmine 2.29[30] after converting the acquired raw data files to an mzXML data format using MSConvert (ProteoWizard). First, *m/z* features were detected using the centroid algorithm followed by a chromatogram building step. Resulting chromatograms were deconvoluted using the noise amplitude algorithm. Further simplification occurred by deisotoping, keeping the lowest *m/z* value as the representative isotope. During the deisotoping, chromatographic peaks were also filtered according to peak width: only peaks with a width between 0.05 and 1 minute were retained. Next, peaks were aligned across samples using the random sample consensus (RANSAC) alignment algorithm. Finally, using the same RT and *m/z* range gap filler algorithm, any missing peaks were re-iteratively extracted. The obtained *m/z* features were then imported in R and processed using an in-house developed script.[31] In short, fold changes between samples and negative controls were calculated. Secondly, a volcano plot

was created to plot the p-value from a student t-test as a function of the calculated fold change for each of the *m/z* features; an example can be found in Figure 1. Features with a p-value <0.05 and a log 10-fold change >10 were selected for further identification using the same criteria as described in subsection 2.5.5. The Generate Formulas algorithm in the MassHunter Qualitative Analysis software (version B.07.00, Agilent Technologies, Santa Clara, CA, USA) was used to predict the corresponding molecular formulas.

2.5.3 | Mass profiler professional workflow

Features were extracted using the Find by Molecular Feature algorithm in MassHunter Qualitative Analysis software (version B.07.00, Agilent Technologies, Santa Clara, CA, USA). Restrictions for *m/z* and retention time were set to *m/z* 50–700 and 1–16.5 minutes, respectively. The resulting data were imported in Mass Profiler Professional (version 12.5, Agilent Technologies, Santa Clara, CA, USA). Samples were grouped per type (positive/negative control, replicate), incubation time (1 or 3 hours) for phase I experiments, and reaction type (Gluc or Sulf) for phase II experiments.

After alignment, features were filtered by frequency to eliminate all entities that were present in one or more of the negative controls. Remaining features were selected for further identification using the same criteria as described in subsection 2.5.5 and molecular formulas were generated using the Generate Formulas algorithm in the MassHunter Qualitative Analysis software (version B.07.00, Agilent Technologies, Santa Clara, CA, USA).

2.5.4 | *In vivo* sample data analysis

The urine sample was analyzed using a suspect screening workflow as described in subsection 2.5.1. The database of possible biotransformation products was updated with the biotransformation products identified via the *in vitro* metabolism experiments using the non-target screening workflows.

2.5.5 | Identification of the biotransformation products

For all workflows, identification of the biotransformation products was based on the accurate mass and isotopic profile obtained in the MS mode and on the fragmentation pattern of product ions and their accurate mass, with the following criteria: (a) a maximal mass variation of ±10 ppm between the measured and theoretical parent ions; (b) a maximal mass variation of ±25 ppm for product ions; (c) the measured isotope pattern matched with the predicted ones with an isotope abundance score of at least 70; (d) the identified biotransformation products were not present in any of the negative control samples; and (e) the detected biotransformation products were present in at least two out of three replicates.

3 | RESULTS AND DISCUSSION

3.1 | Experimental quality controls

MS and MS/MS spectra of the identified biotransformation products of phenacetin and 4-NP were found as expected and are showed in the supporting information (Figures SI – 3 to SI – 7).

3.2 | 5Cl-THJ-018 (parent drug)

The parent compound was detected in positive ionization mode ($[M + H]^+$, *m/z* 377.1417). Figure 2 shows the MS/MS spectrum and fragmentation pattern of 5Cl-THJ-018. Loss of the naphthalene group resulted in a product ion at *m/z* 249.0789. Further loss of hydrogen

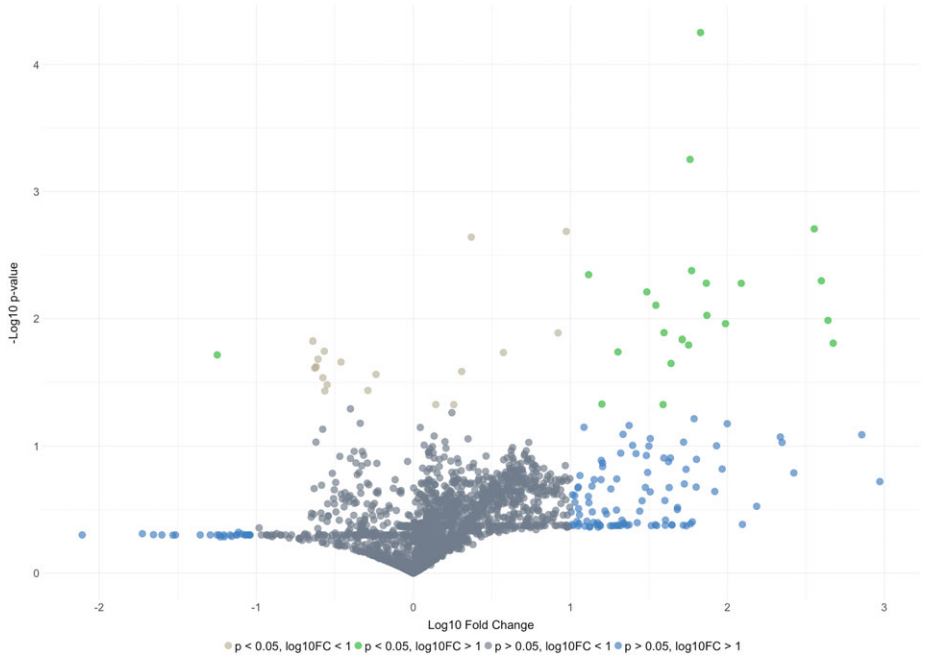

FIGURE 1 Volcano plot of *m/z* values in samples of phase I metabolism after 3 hours of incubation. Features are colored in function of the combination of their respective p-value and fold change. Features of interest were colored in green (p > 0.05 and absolute $\log_{10}$ fold change >10) [Colour figure can be viewed at wileyonlinelibrary.com]

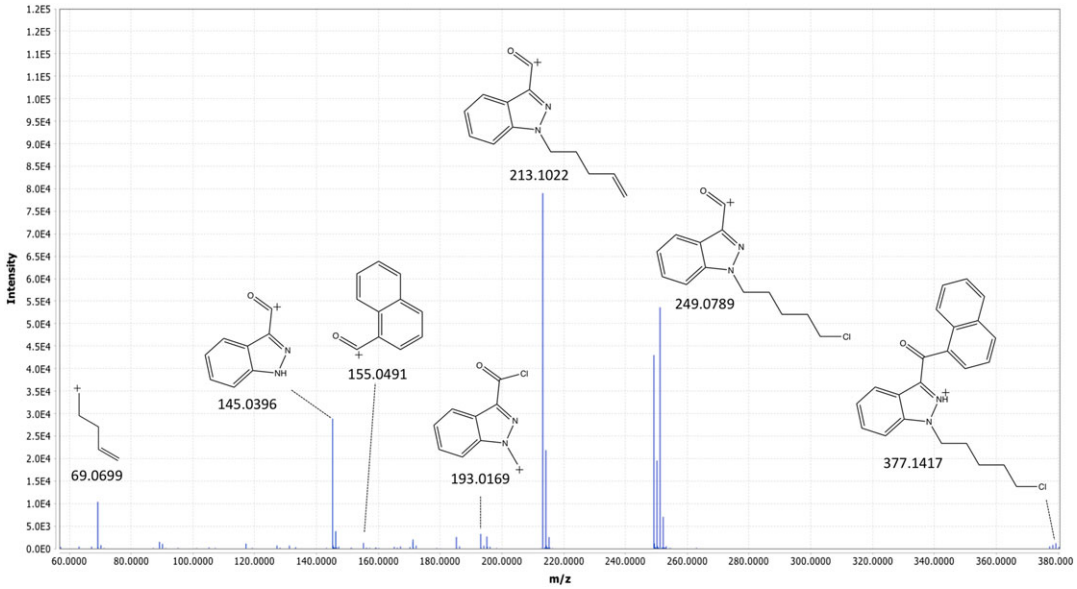

FIGURE 2 MS/MS spectrum with product ions of 5Cl-THJ-018 [Colour figure can be viewed at wileyonlinelibrary.com]

chloride suggested the formation of the product ion at *m/z* 213.1022. The production ion *m/z* 145.0396 was explained by the loss of the naphthalene moiety and pentyl chain. Product ions at *m/z* 155.0491 and *m/z* 69.0699 corresponded to the naphthalene structure with the carbonyl residue and the pentyl chain. A chlorine rearrangement of the structure, similar to the fluorine rearrangement described by Diao et al,[13] led to *m/z* 193.0169. Injection of an analytical standard confirmed the identification of 5Cl-THJ-018.

3.3 | Phase I biotransformation products

An overview of all identified *in vitro* biotransformation products can be found in Table 1. Figure 3 shows the time profiles of the biotransformation products while Figure 4 presents an overview of the elucidated potential metabolic pathway.

3.3.1 | Oxidative dechlorination and further oxidation

M16 corresponded to the oxidative dechlorination of 5Cl-THJ-018. Product ions at *m/z* 145.0406 and *m/z* 155.0489 were common product ions with the parent compound, excluding hydroxylation on the naphthalene or indazole moiety. Subsequent loss of the naphthalene and water resulted in product ions at *m/z* 231.1100 and 213.1025. Three different pathways were further promoted from M16: hydroxylation of the naphthalene residue (M4), aldehyde formation (M18) and a naphthalene dihydrodiol (M5) formation.

M4 consisted of four isomers, eluting between 8.50 and 10.86 minutes in positive ionization mode. Product ions at *m/z* 213.0986 and 145.0413 were already described for the parent compound. The absence of a product ion with *m/z* 155.0489 and the presence of *m/z* 171.0424 confirmed the hydroxylation of M16 on the naphthalene structure. Further hydroxylation of M4 on the naphthalene resulted in M9. Loss of water and dihydroxynaphthalene resulted in the product ions at *m/z* 373.1564 and 231.1128, respectively. M3 was formed due to oxidative dechlorination, hydroxylation of the naphthalene and three hydroxylations on the pentyl-chain. M3 was identified in positive ionization mode and consisted of two isomers. Product ions at *m/z* 389.1485 and 371.1347 corresponded to the loss of one and two water molecules, respectively.

Oxidation of M16 led to the formation of the corresponding aldehyde M18. The double bound equivalent (DBE) of 15 corresponded with the proposed formula ($C_{23}H_{20}N_2O_2$). Loss of the naphthalene structure resulted in the product ion *m/z* 229.0897. The carboxylic acid (M15) derived from M18. Identification was confirmed based on the presence of *m/z* 355.1485 after loss of water as also observed by Diao et al.,[13] *m/z* 245.0932 due to loss of the naphthalene structure and *m/z* 217.0978 which corresponds to the indazole and carboxylated pentyl side chain. The product ion at *m/z* 155.0511 corresponded to the naphthalene. Hydroxylation of M15 led to four isomers of M2 eluting between 8.43 and 10.73 minutes. The lack of product ion *m/z* 155.0511 and the presence of *m/z* 171.0452 confirmed the hydroxylation on the naphthalene moiety.

The two isomers of M5 eluted at 8.50 and 8.56 minutes. The product ion at *m/z* 231.1111 corresponded to the formation of a dihydrodiol structure on the naphthalene structure. M5 also shared product ions *m/z* 213.1000 and 145.0403 with M16.

3.3.2 | Chlorinated biotransformation products

Similarly to the above described biotransformation of M16, consecutive hydroxylation of the parent compound led to several chlorinated phase I biotransformation products. One set of biotransformation products originated from the formation of a naphthalene dihydrodiol (M13), eluting at 11.50 minutes. Loss of water resulted in *m/z* 393.1371. Product ions *m/z* 213.1006 and *m/z* 145.0385 were shared with the parent compound. A product ion at *m/z* 249.0772 (also shared with the parent compound) confirmed the presence of the dihydrodiol function on the naphthalene moiety. Further

TABLE 1 Metabolite ID, metabolic pathway, indication if metabolite was identified in the *in vivo* sample, retention time, data analysis workflow for identification, level of confirmation according to Schymanski et al,[40] molecular formula, exact mass, parent ion detected, mass difference and MS/MS product ions of biotransformation products identified in the *in vitro* metabolism assay. Level 1 (L1): Confirmed structure by reference standard; level 2a (L2a): Probable structure by library spectrum match; level 3 (L3): Tentative candidate based on experimental data; level 4 (L4): Unequivocal formula based on MS1 and isotope ratios. *a: Confirmed using results from Diao et al[13]; B: Confirmed using mzCloud.Org. #: +: Detected in ESI+; −: Detected in ESI-

ID	Metabolic Pathway	Identified *in vivo*	RT (min)	Workflow	Level of Confirmation*	Molecular Formula	Exact Mass	Parent Ion (*m/z*) #	Δ Mass (ppm)	MS/MS Product Ions
Parent			15.03	All	L1	C23H21ClN2O	376.1342	377.1417 $^{+}$	−0.94	249.0789; 213.1022; 193.0169; 155.0491; 145.0396; 69.0699
M01-A	Oxid. Dechlorination + dihydrodiol formation + glucuronidation		7.48	MzMine	L3	C29H32N2O10	568.2057	569.2146 $^{+}$	1.81	375.1772; 357.1599; 231.1142; 213.1030; 175.0458; 145.0341; 69.0708
M01-B	Oxid. Dechlorination + dihydrodiol formation + glucuronidation		8.10	MzMine	L3	C29H32N2O10	568.2057	569.2142 $^{+}$	1.23	375.1772; 357.1599; 231.1142; 213.1030; 175.0458; 145.0341; 69.0708
M02-A	Oxid. Dechlorination to COOH + hydroxylation	X	8.43	All	L2a^{A}	C23H20N2O4	388.1423	389.1511 $^{+}$	2.53	371.1409; 343.1425; 245.0968; 227.0833; 217.0971; 171.0452; 145.0473
M02-B	Oxid. Dechlorination to COOH + hydroxylation	X	8.77	All	L2a^{A}	C23H20N2O4	388.1423	389.1529 $^{+}$	7.16	371.1349; 343.1586; 245.0913; 227.0825; 217.0995; 171.0448; 145.0290
M02-C	Oxid. Dechlorination to COOH + hydroxylation	X	10.46	All	L2a^{A}	C23H20N2O4	388.1423	389.1533 $^{+}$	8.07	245.0968; 231.1082; 213.0972; 171.0404; 145.0380; 69.0696
M02-D	Oxid. Dechlorination to COOH + hydroxylation	X	10.73	All	L2a^{A}	C23H20N2O4	388.1423	389.1513 $^{+}$	2.97	371.1370; 245.0951; 227.0840; 217.0962; 171.0414; 145.0420
M03-A	Oxid. Dechlorination + hydroxylation	X	8.43	Target/MzMine	L2a^{A}	C23H22N2O5	406.1529	407.1619 $^{+}$	2.80	389.1485; 371.1347; 343.1321; 245.0924; 227.0784; 217.0921; 171.0424; 145.0387
M03-B	Oxid. Dechlorination + hydroxylation	X	8.77	Target/MzMine	L2a^{A}	C23H22N2O5	406.1529	407.1615 $^{+}$	1.91	389.1485; 371.1347; 343.1321; 245.0924; 227.0784; 217.0921; 171.0424; 145.0387
M04-A	Oxid. Dechlorination + hydroxylation		8.50	All	L2a^{A}	C23H22N2O3	374.1630	375.1723 $^{+}$	3.83	357.1629; 231.1074; 213.0986; 171.0403; 145.0387; 69.0689
M04-B	Oxid. Dechlorination + hydroxylation		8.86	All	L2a^{A}	C23H22N2O3	374.1630	375.1706 $^{+}$	−0.63	357.1639; 231.1154; 213.1029; 171.0403; 145.0413; 69.0704
M04-C	Oxid. Dechlorination + hydroxylation		10.45	All	L4	C23H22N2O3	374.1630	375.1744 $^{+}$	9.4	NA
M04-D	Oxid. Dechlorination + hydroxylation		10.62	All	L4	C23H22N2O3	374.1630	375.1707 $^{+}$	−0.38	NA
M04-E	Oxid. Dechlorination + hydroxylation		10.86	All	L2a^{A}	C23H22N2O3	374.1630	375.1711 $^{+}$	0.72	231.1067; 213.0955; 145.0427; 69.0677
M05-A	Oxid. Dechlorination + dihydrodiol formation		8.50	Target/ MPP	L2a^{A}	C23H24N2O4	392.1736	393.1827 $^{+}$	3.35	231.1111; 213.1000; 175.0521; 145.0403
M05-B	Oxid. Dechlorination + dihydrodiol formation		8.86	Target/ MPP	L2a^{A}	C23H24N2O4	392.1736	393.1820 $^{+}$	1.50	231.1111; 213.1000; 175.0521; 145.0403
M06	Oxid. Dechlorination + hydroxylation + glucuronidation		8.99	All	L3	C29H30N2O10	566.1900	567.1970 $^{+}$	−1.51	391.1603; 231.1099; 213.0988; 145.0371

(Continues)

TABLE 1 (Continued)

ID	Metabolic Pathway	Identified *in vivo*	RT (min)	Workflow	Level of Confirmation*	Molecular Formula	Exact Mass	Parent Ion (*m/z*) #	Δ Mass (ppm)	MS/MS Product Ions
M07-A	Oxid. Dechlorination to COOH + glucuronidation	X	9.00	Target	L3	C29H28N2O9	548.1795	549.1920 $^{+}$	8.54	421.2307; 373.1783; 355.1600; 245.1058; 155.0572
M07-B	Oxid. Dechlorination to COOH + glucuronidation	X	10.10	Target	L3	C29H28N2O9	548.1795	549.1878 $^{+}$	0.85	421.2307; 373.1783; 355.1600; 245.1058; 155.0572
M08	Hydroxylation + glucuronidation		9.41	MzMine	L3	C29H29ClN2O10	600.1511	601.1592 $^{+}$	0.46	425.1160; 265.0687; 145.0340
M09	Oxid. Dechlorination + hydroxylation		10.39	All	L3	C23H22N2O4	390.1580	391.1664 $^{+}$	1.42	373.1564; 231.1128; 213.1054; 175.0505; 145.0416
M10	Hydroxylation		10.84	MzMine/ MPP	L3	C23H21ClN2O4	424.1190	425.1258 $^{+}$	−2.45	265.0726; 145.0380
M11	Hydroxylation + glucuronidation		11.00	Target	L4	C29H29ClN2O9	584.1562	585.1655 $^{+}$	2.54	NA
M12-A	Hydroxylation		11.47	MzMine	L3	C23H21ClN2O2	392.1292	393.1409 $^{+}$	9.9	249.0835; 213.1055; 145.0504
M12-B	Hydroxylation		12.71	MzMine	L3	C23H21ClN2O2	392.1292	393.1364 $^{+}$	−1.47	265.0825; 155.0521; 145.0423; 85.0645; 67.0555
M13	Dihydrodiol formation		11.47	All	L3	C23H23ClN2O3	410.1397	411.1491 $^{+}$	3.81	393.1371; 249.0741; 213.0974; 145.0385; 69.0666
M14	N-dealkylation		11.60	Target	L2a^{A}	C18H12N2O	272.0950	273.1040 $^{+}$	4.29	145.0361
M15	Oxid. Dechlorination to COOH	X	11.90	Target	L2a^{B}	C23H20N2O3	372.1474	373.1552 $^{+}$	0.04	355.1485; 245.0932; 227.0863; 217.0978; 155.0511; 127.0556
M16	Oxid. Dechlorination	X	12.12	All	L2a^{B}	C23H22N2O2	358.1681	359.1762 $^{+}$	0.87	341.1889; 231.1100; 213.1063; 155.0874; 145.0399; 127.0397
M17	Hydroxylation		12.82	Target/MzMine	L3	C23H21ClN2O3	408.1241	409.1326 $^{+}$	1.77	249.0765; 213.0978; 193.0144; 145.0370
M18	Oxid. Dechlorination to aldehyde		12.89	MzMine	L2a^{A}	C23H20N2O2	356.1525	357.1624 $^{+}$	5.69	229.0897; 145.0398
M19	Dihydrodiol formation + hydroxylation		6.57	MzMine	L4	C23H23ClN2O5	442.1295	441.1231 $^{-}$	3.15	NA
M20	Oxid. Dechlorination to COOH + hydroxylation + sulfation	X	6.66	MzMine/ MPP	L3	C23H20N2O8S	484.0940	483.0880 $^{-}$	2.58	403.1272; 359.1400; 303.0759; 159.0436; 79.9560
M21	Oxid. Dichlorination + hydroxylation + sulfation		7.60	MPP	L3	C23H22N2O8S	486.1097	485.1030 $^{-}$	0.99	405.1448; 219.1107; 159.0458; 117.0448; 80.9645
M22	Oxid. Dichlorination + hydroxylation + sulfation		8.60	MzMine/ MPP	L3	C23H22N2O7S	470.1148	469.1077 $^{-}$	0.29	389.1483; 203.1140; 159.0447; 117.0449; 80.9679
M23-A	Dihydrodiol formation + hydroxylation		9.32	MPP	L4	C23H23ClN2O4	426.1346	425.1295 $^{-}$	6.43	NA
M23-B	Dihydrodiol formation + hydroxylation		10.15	MPP	L4	C23H23ClN2O4	426.1346	425.1281 $^{-}$	3.22	NA

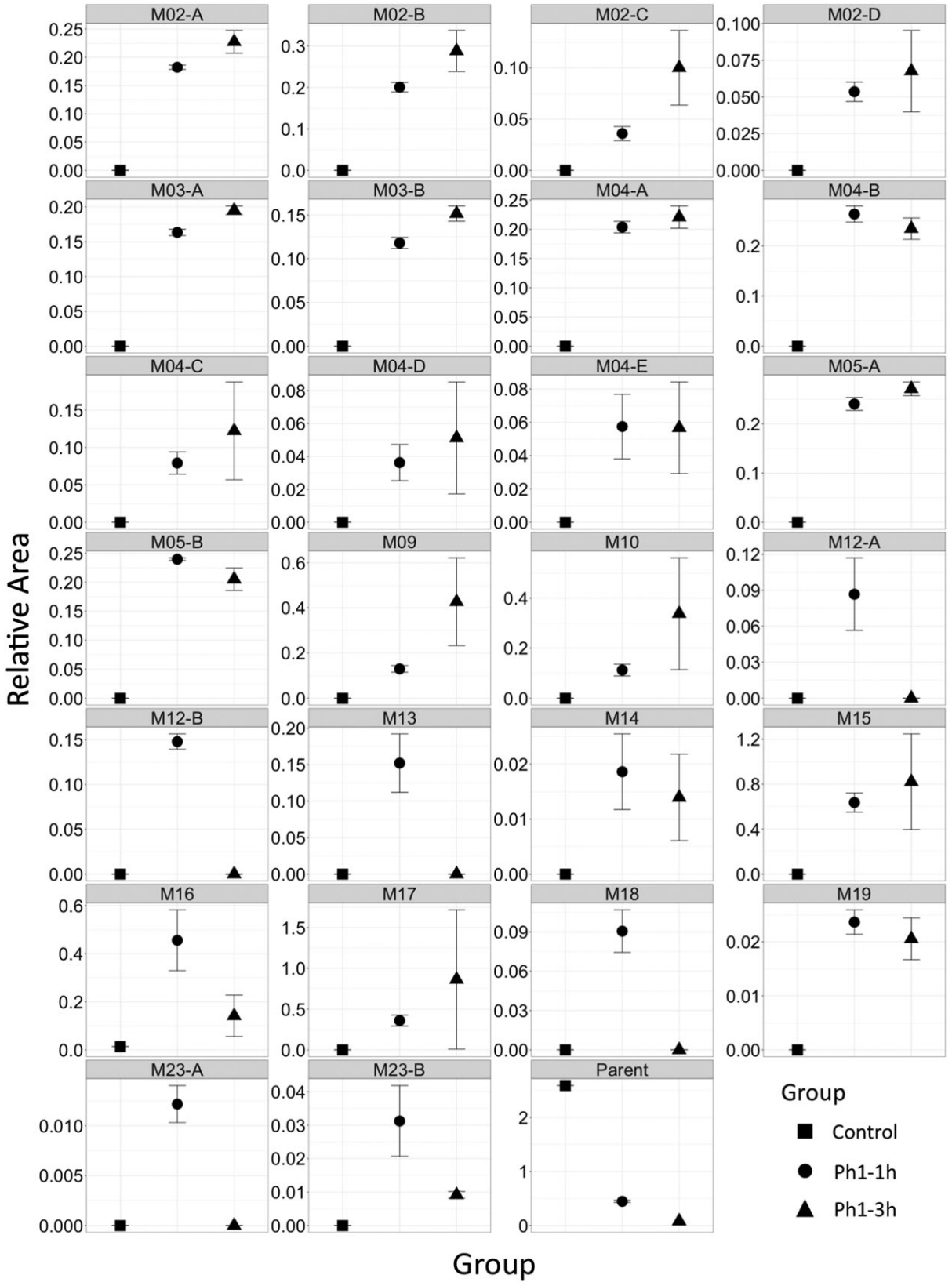

FIGURE 3 Overview of the relative areas (with standard deviation) of all *in vitro* biotransformation products of 5Cl-THJ-018 identified in the phase I metabolism using the *in vitro* HLM assay

hydroxylation resulted in M23, which was detected in negative ionization mode only. Product ions were not acquired for this compound but the molecule was tentatively identified based on the exact mass and the isotope pattern. Although the obtained data could not confirm the position of the hydroxylation on the pentyl chain, Diao et al previously described for fluorinated SCs that the hydroxylation in monohydroxylated biotransformation products (with retention of the halogen) occurs primarily at ω-1-fluoropentyl.[12]

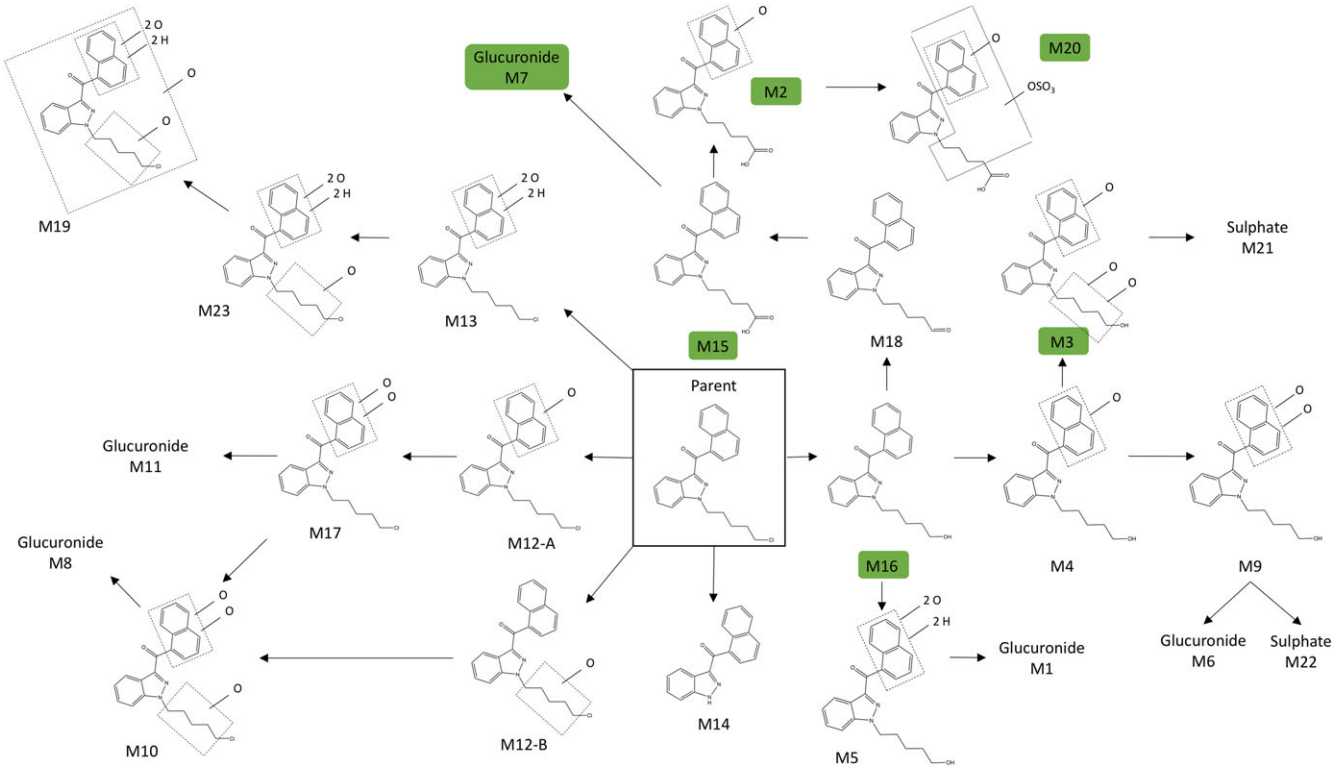

FIGURE 4 Proposed *in vitro* metabolic pathways of 5Cl-THJ-018. *In vitro* biotransformation products found in the *in vivo* sample are marked in green [Colour figure can be viewed at wileyonlinelibrary.com]

Also in the negative ionization mode only, the chromatographic peak at 6.57 minutes could be tentatively attributed to M19, based on the exact mass and corresponding isotope pattern. As M19 originates from the hydroxylation of M23, this further strengthens the positive identification of the latter. Where M5 represents a dechlorinated analogue of M23, no such analogue for M19 has been identified in this study.

Hydroxylation of the parent compound suggested a second set of biotransformation products, starting from the intermediate metabolite M12, the chlorinated analogue of M16. Two isomers of this compound could be chromatographically distinguished, suggesting the hydroxylation occurred on either the naphthalene or the alkyl chain. This was confirmed by the presence of product ions at *m/z* 249.0835 and *m/z* 265.0825. The former represents the loss of the naphthalene carrying the hydroxyl group. The latter originates from the loss of the naphthalene, with the oxygen on the alkyl chain as indicated by the added weight of 16. The indazole-3-carboxaldehyde core showed the common product ion *m/z* 145.0504. Further hydroxylation on the naphthalene or the alkyl chain resulted in the formation of M17. Based on the tentative identification of phase II metabolite M11 (see further) and the presence of product ion at *m/z* 249.0765 (consistent with the loss of $C_{10}H_7O_2$), it is deemed more likely that both hydroxyl functions are located on the naphthalene. It should however be noted that analogy with M4 would suggest a hydroxylation on both the naphthalene moiety and the alkyl chain. A third consecutive hydroxylation led to the formation of M10. Loss of the double hydroxylated naphthalene explains the occurrence of the product ion at *m/z* 265.0726, the chlorinated analogue of M9 product ion at *m/z* 231.1128.

3.3.3 | N-dealkylation

M14 was detected as the protonated molecule at *m/z* 273.1040. Product ion at *m/z* 145.0361 corresponded with the indazole structure. Based on the MS/MS fragmentation pattern and DBE, M14 was identified as the N-dealkylated product of 5Cl-THJ-018.

3.4 | Phase II biotransformation products

Five glucuronidated and three sulfated conjugates were identified. M1 was identified as the glucuronidated product of M5 and consisted of two isomers. Product ions at *m/z* 375.1772 and 357.1599 corresponded to the loss of O-Gluc and the subsequent loss of water respectively. M9 was metabolized to the glucuronidated-(M6) and sulfated-(M22) during phase II metabolism. M6 showed the product ion at *m/z* 391.1603, which corresponds with the loss of the glucuronide. M22 was detected in negative ionization mode as the deprotonated molecule ($[M\text{-}H]^-$, *m/z* 469.1079). Product ions at *m/z* 80.9679 and 389.1483 corresponded to the sulfate and the loss of the conjugated sulfate. The product ion at *m/z* 203.1140 corresponds with the indazole and hydroxylated pentyl chain. The dihydroxylated naphthalene fragment gave rise to *m/z* 159.0447. Thus, no definite structural position of the sulfate could be identified.

M7 was formed after the conjugation of M15 with a glucuronide at the carboxylic acid and suggested two glucuronidated isomers, a carboxylic acid conjugate and a N^+-glucuronide of the aromatic tertiary amine group.[32] Product ions at *m/z* 355.1600, 245.1058 and 155.0472 were already observed for M15. Loss of the naphthalene

resulted in *m/z* 421.2307. Loss of the glucuronide and O-glucuronide resulted in product ions at *m/z* 373.1783 and 355.1600.

Sulfo-conjugation of M3 led to metabolite M21 ($[M\text{-}H]^-$, *m/z* 485.1026). The product ions at *m/z* 405.1448 was formed after loss of the sulfate.

Similar to M9, the chlorinated metabolite M10 was further biotransformed through glucuronidation to M8. Once more the common product ion at *m/z* 145.0340 representing the indazole-3-carboxaldehyde core was present. The position of the glucuronide could not be determined as the product ion at *m/z* 265.0687 represents the loss of the naphthalene either carrying the glucuronide or following previous deglucuronidation (product ion at *m/z* 425.1166).

M11 was found to be the glucuronidated phase II metabolite of M17. However, this compound could only be tentatively identified as MS/MS spectra were not acquired. Neither had an analogous dechlorinated phase II metabolite been found.

3.5 | Time trends of the biotransformation products

Figure 3 shows the relative area of the biotransformation products after 1 hour and 3 hours of phase I incubation. The relative area was calculated by dividing the peak area of the metabolite by the peak area of the internal standard. These data were used to help elucidating the biotransformation pathway shown in Figure 4. Biotransformation products that showed an increase in signal after 1 hour and a decrease in signal after 3 hours of incubation were considered as intermediate products. M12, M13, and M18 are examples of biotransformation products with this specific time trend and could be explained by further metabolization of these compounds to M17, M23, and M15 respectively. M2, M3, M9, and M10 showed an increase in relative area over time, which could be explained by terminal biotransformation products. After 3 hours of incubation, M15, M17, M9, and M10 were the major phase I biotransformation products based on their relative area.

3.6 | Comparison of *in vitro* and *in vivo* data

A new database was compiled for the suspect screening of the urine sample based on the prediction by Meteor Software and updated with the biotransformation products identified using the non-target screening workflows applied in the *in vitro* metabolism experiment. The urine sample was analyzed using a suspect screening workflow and the same criteria as used for the analysis of the *in vitro* experiments (subsection 2.5.5). This resulted in the detection and identification of six metabolites. The favored *in vivo* metabolic pathway appeared to be the oxidative dechlorination (leading to the formation of M16). Consecutive carboxylation and hydroxylation led to the identification of M15 and M2, respectively. The intermediate aldehyde (M18) could not be identified in the urine sample. Detected phase II biotransformation products included M7 (glucuronidation of M15) and M20 (sulfation of M2). Evidence for the presence of M3, a dechlorinated tetrahydroxylated analogue of the parent compound and downstream metabolite of M16, was found as well. However, its precursor M4 has not been detected and neither were the other biotransformation products originating from M4 (M6, M9, or M22). Based on the areas M3, M2, and M15 appeared to be major *in vivo* biotransformation products.

None of the chlorinated biotransformation products were found in the *in vivo* sample. Several studies have reported oxidative dehalogenation as the major metabolism pathway *in vivo* of SCs halogenated at the 5-pentyl position.[12,33,34] Diao et al previously reviewed

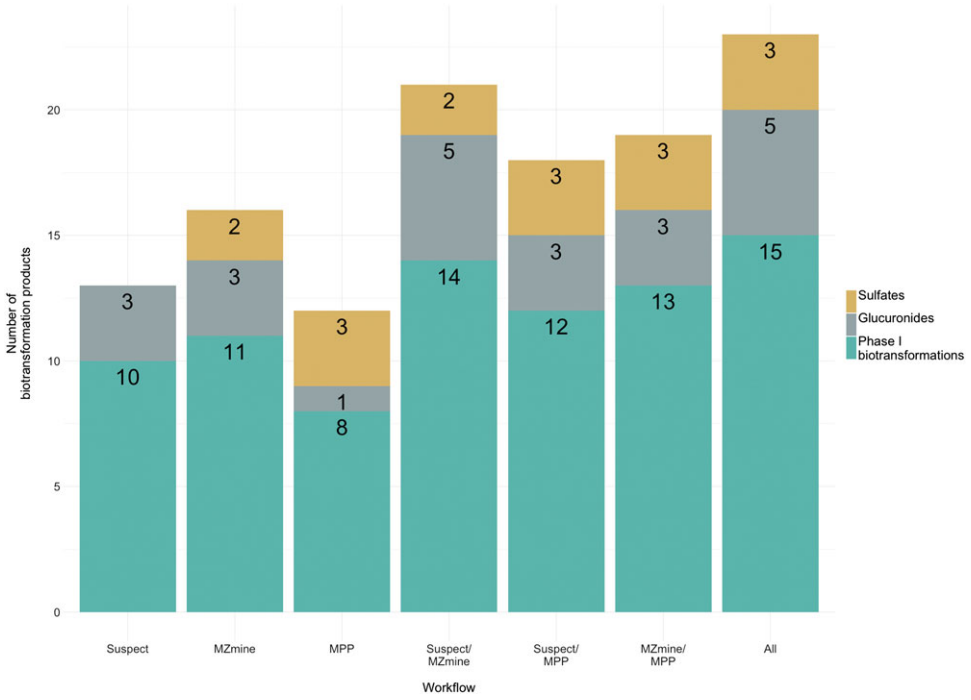

FIGURE 5 Comparison of biotransformation products identified using a combination of different workflows for data analysis. Per workflow identified phase I biotransformations are colored in green, glucuronides in grey, and sulfates in yellow [Colour figure can be viewed at wileyonlinelibrary.com]

studies concerning authentic human urine specimens for the synthetic cannabinoids AM-2201 and 5F-AKB-48.[12] HLMs are rich in some oxidases (CYP450 and flavin-containing monooxygenases) but lack non-CYP450 oxidases present in cytosolic fractions such as alternative oxidase (AOX). As the predominant defluorination is catalyzed by non-CYP450 enzymes, the results from HLM incubation are biased.[12] A similar outcome was observed in our study for the oxidative dechlorination. It should also be mentioned that this study was limited to only one urine sample without knowing the interval between 5Cl-THJ-018 intake and urine collection. During this interval, possible intermediate *in vivo* biotransformation products could have already been further metabolized leading to the apparent absence of these products in the urine sample. Secondly, no deconjugation step was included before LC–QTOF–MS analysis in order to detect the conjugated metabolites. This could however bias the detection of phase I biotransformation products as they could be conjugated.

3.7 | Comparison of 5Cl-THJ-018 to other synthetic cannabinoids

Oxidative dehalogenation of SCs appears to be one of the major pathways and was also present in our study as M15, M16, and M9 were the major identified biotransformation products. Previous studies investigated the metabolism of other synthetic cannabinoids halogenated at the 5-position of the pentyl chain and have also identified metabolites resulting from oxidative dehalogenation, suggesting this pathway to be major for this group of SCs.[13,17,35-37]

Diao et al investigated the metabolism of THJ-018 and the 5-fluoro analogue THJ-2201.[13] Other described pathways such as N-dealkylation, hydroxylation of the naphthalene group and dihydrodiol formation, as well as their resulting biotransformation products, were also found in our study. However, the *N*-oxide biotransformation product previously reported by Diao et al was not detected in this experiment. This study further identified nine biotransformation products (M1, M7, M8, M9, M10, M15, M17, M20, and M22) which were not reported by Diao et al.[13]

Indole-hydroxylated biotransformation products were previously described for JWH-018 (the indole-analogue of THJ-018); however no indazole-hydroxylated products of 5Cl-THJ-018 were identified.[6] These findings confirm the results of the study by Diao et al.[13]

Although this study identified several biotransformation products resulting from the phase II sulfation, UGT-mediated conjugation with glucuronic acid seemed to be of higher importance given the higher number of glucuronides identified *in vitro*. These results are in line with earlier studies regarding the phase II metabolism of synthetic cannabinoids.[11,13,17,35,38,39]

3.8 | Workflow evaluations

As described in the Method section, three different data analysis workflows were combined for the identification of the biotransformation products. In total, 23 biotransformation products were identified combining the results from all workflows. Seven biotransformation products were unique for the MZmine + R workflow, five were identified by the suspect-screening workflow only and only two were unique for the Mass Profiler Professional-workflow. An overview of the results can be found in Figure 5. If only the suspect screening workflow had been used, only 13 out of 23 biotransformation products would have been identified, phase I reaction products and glucuronides but no sulfates. Using only the MZmine + R workflow, two out of three sulfates would have been detected but a total of seven biotransformation products would not have been identified. The Mass Profiler Professional workflow was the only workflow capable of detecting all sulfates, but if only this workflow would have been applied the number of detected phase I reaction products and glucuronides would have been lower resulting in the lowest number of identified products. Only by combining the results from all workflows all four major metabolites (M15, M17, M9, and M10) could be identified. M15 was only identified by suspect screening although the signal intensity was above the threshold for non-target screening. M10 could only be identified using non-target screening as the Meteor Software did not predict this metabolite. Combining suspect screening with the MZMine + R workflow resulted in the highest amount of identified biotransformation products when combining two different workflows. Adding the MPP workflow to this combination added one more phase I reaction product and one more sulfate to the biotransformation product list. These data clearly show the added value of combining suspect analysis with non-targeted screening workflows.

4 | CONCLUSIONS

This study identified 23 biotransformation products of the synthetic cannabinoid 5Cl-THJ-018, of which 15 were phase I and 8 were phase II products formed through hydroxylation, oxidative dechlorination, dihydrodiol formation, and conjugation pathways. To the best of our knowledge, this is the first study identifying the *in vitro* and *in vivo* metabolites of 5Cl-THJ-018. The combination of suspect and non-target screening workflows improved the number of identified biotransformation products. Suspect screening of an authentic urine sample showed that the predominant *in vivo* pathway is through oxidative dechlorination with subsequent hydroxylation and conjugation with glucuronic acid.

ACKNOWLEDGEMENTS

Olivier Mortelé acknowledges funding (GOA project) by the University of Antwerp (UA, Belgium). Celine Gys acknowledges a PhD fellowship from the Research Foundation Flanders (FWO) through project G0E5216N. Philippe Vervliet acknowledges a PhD fellowship from the Research Foundation Flanders (FWO) through project G089016N. This work was also supported by the EU H2020 MASSTWIN (Research and Innovation Program under grant agreement no. 692241). Alexander van Nuijs acknowledges the Research Foundation Flanders (FWO) for his post-doctoral fellowship. Foon Yin Lai acknowledges the EU H2020 Marie Skłodowska-Curie Individual Fellowship (project no. 749845 APOLLO).

CONFLICT OF INTEREST

The authors declare they have no conflict of interest.

ORCID

Philippe Vervliet http://orcid.org/0000-0003-2644-6820
Olivier Mortelé http://orcid.org/0000-0002-6366-2154
Kristof Maudens http://orcid.org/0000-0003-0924-7168
Adrian Covaci http://orcid.org/0000-0003-0527-1136
Alexander L.N. van Nuijs http://orcid.org/0000-0002-9377-6160

REFERENCES

1. EMCDDA. *European Drug Report 2017: Trends and Developments*. Luxembourg: Publications Office of the European Union; 2017.
2. Elsohly MA, Gul W, Wanas AS, Radwan MM. Synthetic cannabinoids: analysis and metabolites. *Life Sci*. 2014;97(1):78-90.
3. Auwarter V, Dresen S, Weinmann W, Muller M, Putz M, Ferreiros N. 'Spice' and other herbal blends: harmless incense or cannabinoid designer drugs? *J Mass Spectrom*. 2009;44(5):832-837.
4. EMCDDA. *New psychoactive substances in Europe. An update from the EU Early Warning System (March 2015)*. Luxembourg: Publications Office of the European Union; 2015.
5. Castaneto MS, Gorelick DA, Desrosiers NA, Hartman RL, Pirard S, Huestis MA. Synthetic cannabinoids: epidemiology, pharmacodynamics, and clinical implications. *Drug Alcohol Depend*. 2014;144:12-41.
6. Chimalakonda KC, Seely KA, Bratton SM, et al. Cytochrome P450-mediated oxidative metabolism of abused synthetic cannabinoids found in K2/spice: identification of novel cannabinoid receptor ligands. *Drug Metab Dispos*. 2012;40(11):2174-2184.
7. Fantegrossi WE, Moran JH, Radominska-Pandya A, Prather PL. Distinct pharmacology and metabolism of K2 synthetic cannabinoids compared to Delta(9)-THC: mechanism underlying greater toxicity? *Life Sci*. 2014;97(1):45-54.
8. Cooper ZD. Adverse effects of synthetic cannabinoids: Management of Acute Toxicity and Withdrawal. *Curr Psychiatry Rep*. 2016;18(5):52.
9. EMCDDA. Two new synthetic cannabinoids to be placed under control across the EU: council implementing decision to control ADB-CHMINACA and CUMYL-4CN-BINACA Lisbon 2018 [updated 14/05/2018. Available from: http://www.emcdda.europa.eu/news/2018/3/council-implementing-decisions-control-adb-chminaca-cumyl-4cn-binaca.
10. Diao X, Carlier J, Zhu M, Huestis MA. Human hepatocyte metabolism of novel synthetic cannabinoids MN-18 and its 5-Fluoro analog 5F-MN-18. *Clin Chem*. 2017;63(11):1753-1763.
11. Sobolevsky T, Prasolov I, Rodchenkov G. Detection of urinary metabolites of AM-2201 and UR-144, two novel synthetic cannabinoids. *Drug Test Anal*. 2012;4(10):745-753.
12. Diao X, Huestis MA. Approaches, challenges, and advances in metabolism of new synthetic cannabinoids and identification of optimal urinary marker metabolites. *Clin Pharmacol Ther*. 2017;101(2):239-253.
13. Diao X, Wohlfarth A, Pang S, Scheidweiler KB, Huestis MA. High-resolution mass spectrometry for characterizing the metabolism of synthetic cannabinoid THJ-018 and its 5-Fluoro analog THJ-2201 after incubation in human hepatocytes. *Clin Chem*. 2016;62(1):157-169.
14. Erratico C, Negreira N, Norouzizadeh H, et al. In vitro and in vivo human metabolism of the synthetic cannabinoid AB-CHMINACA. *Drug Test Anal*. 2015;7(10):866-876.
15. Jang M, Yang W, Shin I, Choi H, Chang H, Kim E. Determination of AM-2201 metabolites in urine and comparison with JWH-018 abuse. *Int J Leg Med*. 2014;128(2):285-294.
16. Sobolevsky T, Prasolov I, Rodchenkov G. Detection of JWH-018 metabolites in smoking mixture post-administration urine. *Forensic Sci Int*. 2010;200(1–3):141-147.
17. Wohlfarth A, Castaneto MS, Zhu M, et al. Pentylindole/Pentylindazole synthetic cannabinoids and their 5-Fluoro analogs produce different primary metabolites: metabolite profiling for AB-PINACA and 5F-AB-PINACA. *AAPS J*. 2015;17(3):660-677.
18. Brandon EFA, Raap CD, Meijerman I, Beijnen JH, Schellens JHM. An update on in vitro test methods in human hepatic drug biotransformation research: pros and cons. *Toxicol Appl Pharmacol*. 2003;189(3):233-246.
19. Fisher MB, Campanale K, Ackermann BL, Vandenbranden M, Wrighton SA. In vitro glucuronidation using human liver microsomes and the pore-forming peptide alamethicin. *Drug Metab Dispos*. 2000;28(5):560-566.
20. Knights KM, Stresser DM, Miners JO, Crespi CL. In vitro drug metabolism using liver Microsomes. *Curr Protoc Pharmacol*. 2016;74:7.8.1-7.8.24.
21. Richter LHJ, Flockerzi V, Maurer HH, Meyer MR. Pooled human liver preparations, HepaRG, or HepG2 cell lines for metabolism studies of new psychoactive substances? A study using MDMA, MDBD, butylone, MDPPP, MDPV, MDPB, 5-MAPB, and 5-API as examples. *J Pharm Biomed Anal*. 2017;143:32-42.
22. Jia L, Liu X. The conduct of drug metabolism studies considered good practice (II): in vitro experiments. *Curr Drug Metab*. 2007;8(8):822-829.
23. Mortele O, Vervliet P, Gys C, et al. In vitro phase I and phase II metabolism of the new designer benzodiazepine cloniprazepam using liquid chromatography coupled to quadrupole time-of-flight mass spectrometry. *J Pharm Biomed Anal*. 2018;153:158-167.
24. Erratico C, Zheng XB, van den Eede N, Tomy G, Covaci A. Stereoselective metabolism of alpha-, beta-, and gamma-Hexabromocyclododecanes (HBCDs) by human liver Microsomes and CYP3A4. *Environ Sci Technol*. 2016;50(15):8263-8273.
25. Ballesteros-Gomez A, Erratico CA, Van den Eede N, Ionas AC, Leonards PEG, Covaci A. In vitro metabolism of 2-ethylhexyldiphenyl phosphate (EHDPHP) by human liver microsomes. *Toxicol Lett*. 2015;232(1):203-212.
26. Negreira N, Erratico C, Kosjek T, et al. In vitro phase I and phase II metabolism of alpha-pyrrolidinovalerophenone (alpha-PVP), methylenedioxypyrovalerone (MDPV) and methedrone by human liver microsomes and human liver cytosol. *Anal Bioanal Chem*. 2015;407(19):5803-5816.
27. Lai FY, Erratico C, Kinyua J, Mueller JF, Covaci A, van Nuijs ALN. Liquid chromatography-quadrupole time-of-flight mass spectrometry for screening in vitro drug metabolites in humans: investigation on seven phenethylamine-based designer drugs. *J Pharm Biomed Anal*. 2015;114:355-375.
28. Negreira N, Erratico C, van Nuijs AL, Covaci A. Identification of in vitro metabolites of ethylphenidate by liquid chromatography coupled to quadrupole time-of-flight mass spectrometry. *J Pharm Biomed Anal*. 2016;117:474-484.
29. Negreira N, Kinyua J, De Brabanter N, Maudens K, van Nuijs AL. Identification of in vitro and in vivo human metabolites of the new psychoactive substance nitracaine by liquid chromatography coupled to quadrupole time-of-flight mass spectrometry. *Anal Bioanal Chem*. 2016;408(19):5221-5229.
30. Pluskal T, Castillo S, Villar-Briones A, Oresic M. MZmine 2: modular framework for processing, visualizing, and analyzing mass spectrometry-based molecular data. *BMC Bioinformatics*. 2010;11(1):395-405.
31. Vervliet P. invitRo - in vitro HLM assay feature prioritizationZenodo. 2018.
32. Hawes EM. N +−Glucuronidation, a common pathway in human metabolism of drugs with a tertiary amine group. *Drug Metab Dispos*. 1996;26(9):830-837.
33. Kanamori T, Kanda K, Yamamuro T, et al. Detection of main metabolites of XLR-11 and its thermal degradation product in human hepatoma HepaRG cells and human urine. *Drug Test Anal*. 2015;7(4):341-345.
34. Jang M, Kim IS, Park YN, et al. Determination of urinary metabolites of XLR-11 by liquid chromatography-quadrupole time-of-flight mass spectrometry. *Anal Bioanal Chem*. 2016;408(2):503-516.
35. Wohlfarth A, Gandhi AS, Pang S, Zhu M, Scheidweiler KB, Huestis MA. Metabolism of synthetic cannabinoids PB-22 and its 5-fluoro analog, 5F-PB-22, by human hepatocyte incubation and high-resolution mass spectrometry. *Anal Bioanal Chem*. 2014;406(6):1763-1780.
36. Richter LHJ, Maurer HH, Meyer MR. New psychoactive substances: studies on the metabolism of XLR-11, AB-PINACA, FUB-PB-22, 4-

methoxy-alpha-PVP, 25-I-NBOMe, and meclonazepam using human liver preparations in comparison to primary human hepatocytes, and human urine. *Toxicol Lett*. 2017;280:142-150.

37. Mogler L, Franz F, Wilde M, et al. Phase I metabolism of the carbazole-derived synthetic cannabinoids EG-018, EG-2201, and MDMB-CHMCZCA and detection in human urine samples. *Drug Test Anal*. 2018;10(9):1417-1429.
38. Kevin RC, Lefever TW, Snyder RW, et al. In vitro and in vivo pharmacokinetics and metabolism of synthetic cannabinoids CUMYL-PICA and 5F-CUMYL-PICA. *Forensic Toxicol*. 2017;35(2):333-347.
39. Mogler L, Franz F, Rentsch D, et al. Detection of the recently emerged synthetic cannabinoid 5F–MDMB-PICA in 'legal high' products and human urine samples. *Drug Test Anal*. 2018;10(1):196-205.
40. Schymanski EL, Jeon J, Gulde R, et al. Identifying small molecules via high resolution mass spectrometry: communicating confidence. *Environ Sci Technol*. 2014;48(4):2097-2098.

SUPPORTING INFORMATION

Additional supporting information may be found online in the Supporting Information section at the end of the article.

How to cite this article: Vervliet P, Mortelé O, Gys C, et al. Suspect and non-target screening workflows to investigate the *in vitro* and *in vivo* metabolism of the synthetic cannabinoid 5Cl-THJ-018. *Drug Test Anal*. 2018;1–13. https://doi.org/10.1002/dta.2508